

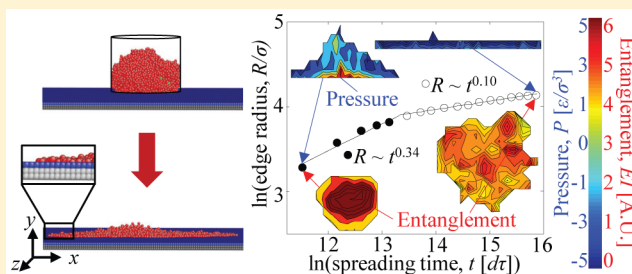
Spreading Kinetics of Ultrathin Liquid Films Using Molecular Dynamics

Brooklyn A. Noble,[†] C. Mathew Mate,[#] and Bart Raeymaekers^{*,†}

[†]Department of Mechanical Engineering, University of Utah, Salt Lake City, Utah 84112, United States

Supporting Information

ABSTRACT: Ultrathin liquid films play a critical role in numerous engineering applications. Although crucial to the design and application of ultrathin liquid films, the physical mechanisms that govern spreading on the molecular scale are not well-understood, and disagreement among experiments, simulations, and theory remains. We use molecular dynamics simulations to quantify the speed at which the edge of a polymer droplet advances on a flat substrate as a function of various environmental and design parameters. We explain the physical mechanisms that drive and inhibit spreading, identify different spreading regimes, and clarify transitions between spreading regimes. We demonstrate that the edge of a droplet spreads according to a power law with two distinct regimes, which we attribute to competing physical mechanisms: a pressure difference in the liquid droplet and molecule entanglement. This research unifies many years of liquid spreading research and has implications for systems that involve designing complex ultrathin liquid films.



INTRODUCTION

Ultrathin liquid films are important in numerous physical phenomena and engineering applications including soil science, lubrication, manufacturing, cosmetics, and food processing, among many others.¹ In particular, micro- and nanoscale systems and devices often rely on ultrathin polymer-based liquid films to reduce surface effects, which become increasingly important with decreasing scale. Examples of such systems include hard disk drives,² micro- and nanoelectromechanical systems,³ microfluidic arrays,⁴ antibiofouling/fouling-release coatings,⁵ and nanoimprint lithography;⁶ these systems are ubiquitous in consumer electronics, medical devices, and microfabrication technologies. How a polymer-based liquid film interacts with and adsorbs onto a surface determines properties such as surface conformation, adherence to a substrate, and reflow of the liquid film into depletion zones, which are often critical to performance during device operation. Therefore, understanding the physical mechanisms that govern how an ultrathin liquid film initially adsorbs onto a surface and spreads can be critical to designing these systems and devices that rely on micro- or nanoscale mechanisms.⁷

The most common experiment to study the spreading kinetics of thin liquid films involves monitoring a liquid droplet, deposited on a flat substrate by a pipet, syringe, or sharp needle, while it spreads with time.⁸ During spreading, the droplet radius R increases with time t and typically obeys a power law $R \sim t^\nu$, where ν is the spreading exponent.⁹ For a macroscale droplet spreading on a surface that it wets, Tanner's law predicts $\nu = 0.1$, for a droplet that retains its shape apart from a change in scale. Tanner's law accounts for the interaction between surface tension and viscous forces.¹⁰

The spreading of a macroscale droplet is typically preceded on the microscale by a precursor film, one or two monolayers thick, which extends out from the central droplet. Two types of theories have been developed for explaining the spreading of these precursor films: (1) A diffusion theory that predicts $\nu = 0.5$ based on Brownian motion of individual molecules where the square displacement $x^2 = 2Dt$ increases linearly with time, and D is the self-diffusion coefficient.^{11,12} Accordingly, several experiments^{12–17} observed $\nu \approx 0.5$ for precursor films of polymer liquids. (2) A recent theory by Liao et al.¹⁸ predicts $\nu = 1/3$ for the precursor film spreading from a microscale droplet. This theory assumes that spreading can be modeled as continuum flow driven by disjoining pressure in the presence of intensified wall slip. Recent experiments by Mate^{19,20} confirm that ν is close to $1/3$ for many polymer liquid films.

In general, however, experiments of droplet spreading do not report a uniform value for ν . Instead, the spreading exponent varies over a wide range of $0.03 \leq \nu \leq 0.32$,²¹ depending on the liquid–solid interaction. These studies also document multiple distinct spreading regimes, typically with an initial spreading exponent $0.31 \leq \nu \leq 1.00$ followed by a slower one $0.1 \leq \nu \leq 0.5$.^{19,20,22,23} The wide range of values for ν may indicate that different spreading mechanisms exist in different situations.

Since experiments become increasingly difficult with decreasing length scale, molecular dynamics (MD) simulations have been employed to study the spreading kinetics of liquids at

Received: January 31, 2017

Revised: March 19, 2017

Published: March 20, 2017

the nanoscale. These MD studies also find a wide range of values for the spreading exponent and report spreading based on either a single spreading exponent ranging from $0.2 \leq \nu \leq 0.5$,^{24–27} two spreading exponents that reveal a fast ($0.4 \leq \nu \leq 1.0$) followed by a relatively slow spreading exponent ($0.5 \leq \nu \leq 0.7$),^{27–29} or even three successively slower spreading exponents, $\nu \approx 0.8$ to $\nu \approx 0.5$ and $\nu \approx 0.1$,²⁷ depending on the simulation techniques and configuration (e.g., two- versus three-dimensional spreading, simple versus chain-like molecules, and variations in droplet size and molecular weight). However, these MD simulations, with widely varying, and sometimes seemingly unrelated results, have not yet provided an explanation that unifies a multitude of reports.

Here, we employ a coarse-grained bead spring (CGBS) MD model to quantify three-dimensional spreading of a liquid polymer droplet on a flat substrate as a function of polymer chain length, polymer quantity, and functional chemical end groups of the polymer and the substrate. Liquid polymer-based films are particularly relevant to micro- and nanoscale applications, and experimental results are abundantly available. We explain the physical mechanisms underlying ultrathin liquid film spreading kinetics, and provide insight into the widely varying experimental results documented in the literature.

Molecular Dynamics Model. We perform MD simulations of a nanoscale liquid polymer droplet spreading on a flat substrate using a CGBS model and the LAMMPS code.^{30,31} The CGBS model averages atomic interactions for computational simplicity yet preserves the essence of the molecular structure. We consider two types of perfluoropolyether (PFPE) polymer commonly used as lubricant in micro- and nanoscale devices, both of which have a backbone structure of $X-[(O-CF_2-CF_2)_p-(O-CF_2)_q]-O-X$ where $(p/q \cong 2/3)$: a Zdol molecule, which terminates with a functional hydroxyl group ($X = CF_2-CH_2-OH$), and a Z molecule, which terminates with a nonfunctional trifluoromethyl group ($X = CF_3$).

Figure 1 shows a schematic of the MD model before and after spreading of the liquid polymer, which consists of

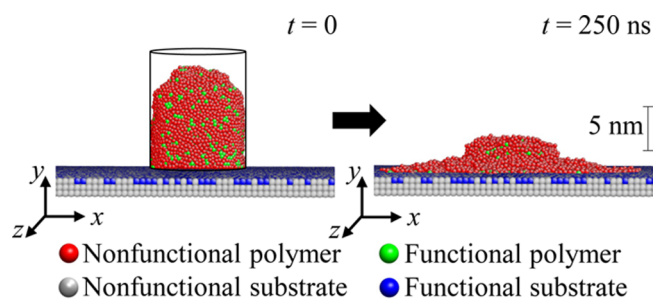


Figure 1. Molecular dynamics simulation before and after spreading of the liquid polymer with functional end groups (Zdol).

backbone beads (red) and terminating functional end beads (green), representing the hydroxyl end group of Zdol. The flat substrate consists of three layers of a rigid, cubic lattice structure composed of nonfunctional beads (gray) and a fraction S_f of functional (blue) beads on the top layer only, which can attract functional polymer end beads (green) and represent a functional hydroxyl group. The potential function interactions^{28,32–34} are similar to validated potentials used in previous research and are discussed in detail in the Supporting Information (SI).

To vary the molecular mass, we vary the polymer molecule length from $10 \leq N \leq 400$ beads for both polymer types, while maintaining a constant bead mass of 0.2 kg/mol. We also vary the quantity of polymer in the simulation from $5000 \leq Q \leq 40\,000$ beads, and the functional substrate fraction from $0\% \leq S_f \leq 100\%$, which defines the fraction of substrate beads that attract functional polymer end beads.

RESULTS AND DISCUSSION

Despite the molecular scale of our simulations, we observe liquid polymer spreading to be most consistent with the concept of continuum flow where a pressure difference drives, and viscosity inhibits flow. This contrasts with many reports that identify diffusion as the driving mechanism of liquid polymer spreading.^{12–17} Specifically, we observe three spreading scenarios: pressure-driven flow characterized by a fast spreading regime; pressure-driven, entanglement inhibited flow characterized by a fast spreading regime followed by a slow spreading regime; and pressure-driven, chemically inhibited flow characterized by a slow spreading regime. Figures 2–4 illustrate the extreme cases considered in this work, and Tables S1–S3 of the SI provide the results for intermediate cases. We also provide videos in the SI to illustrate the evolution of the pressure and entanglement maps, the droplet edge radius, and the side view of the droplet as it spreads with time (Videos S1–S3).

Pressure-Driven Flow. Figure 2 illustrates spreading of liquid Z and Zdol polymer droplets with $S_f = 0\%$, $N = 10$ beads/molecule, and $Q = 10\,000$ polymer beads. Figure 2a shows the droplet edge radius as a function of spreading time. To quantify the spreading exponent ν , we fit straight lines (least-squares method) to data points at 100 000 time-step intervals, where $d\tau$ is one time-step. We simultaneously evaluate the droplet thickness profile to determine whether a central droplet is present (see insets), which we define as a thickness greater than the precursor film thickness of 3σ , where σ is the diameter of one bead.³² In this paper, we adopt the convention in Figures 2–4 that solid and hollow markers indicate that a central droplet is present or has depleted, respectively. We also depict in one of the insets in Figure 2a a molecular view of the precursor film that has spread to a thickness of approximately one bead. From Figure 2a we observe that the central droplet depletes quickly, and spreading with a power exponent $\nu \approx 1/3$ occurs both when the central droplet is present and when it is absent.

Figure 2b shows the pressure difference (ΔP) and the entanglement index (EI) within a droplet as a function of time for the Z polymer with $N = 10$ and $Q = 10\,000$. The pressure difference (ΔP) is defined as the difference in pressure near the substrate (less than 3σ in height) between the outermost 20% and innermost 20% radii of the droplet. The entanglement index (EI) is defined as the average number of beads that remain within 2σ of each other for at least 100 000 time steps.³⁵ We fit a curve to data points at 100 000 time-step intervals yet show markers at 600 000 time-step intervals for clarity. From Figure 2b, we observe that the pressure difference defined in this manner decreases quickly after spreading starts, and approaches zero once the central droplet has depleted. The EI is large at the inception of spreading because a cylinder initially confines the liquid polymer, but when allowed to spread, the short molecules spread freely, causing the EI to decrease immediately. Note that $EI \approx 4$ indicates molecules are largely unentangled, as the presence of persistent contacts from adjacent

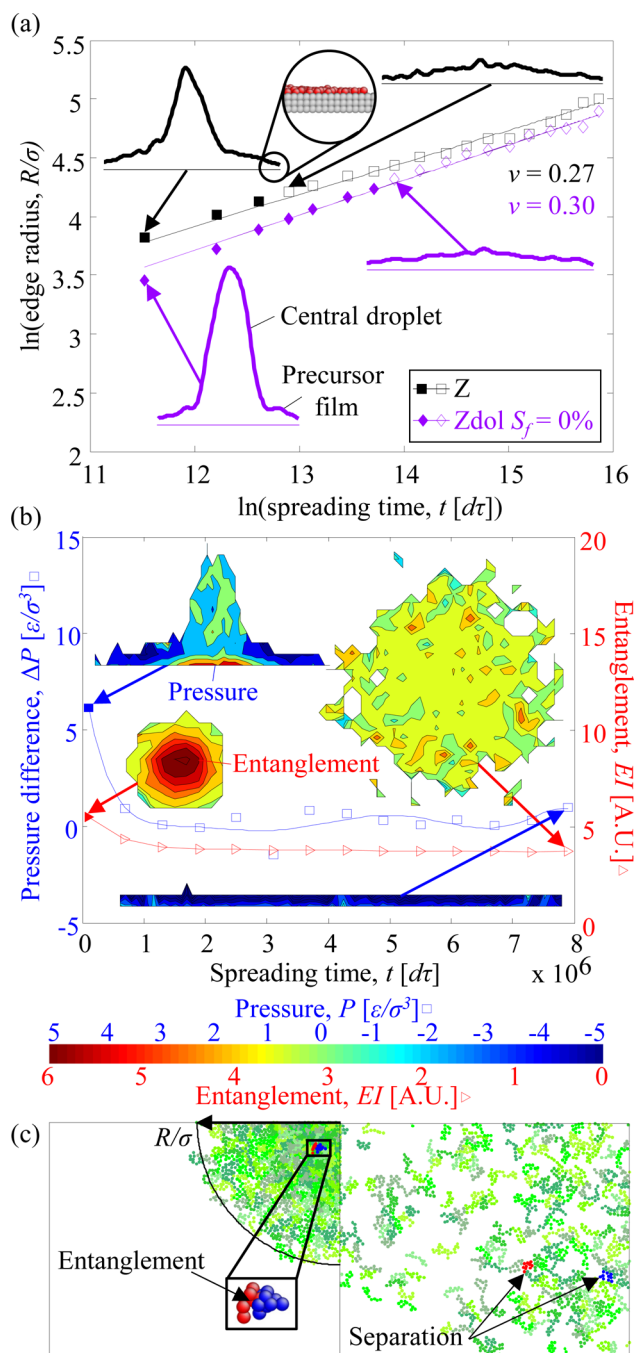


Figure 2. Pressure-driven flow. (a) Edge radius versus spreading time for Z and Zdol ($S_f = 0\%$, $N = 10$ beads/molecule, $Q = 10\,000$ beads). Solid and hollow markers indicate that a central droplet exists or has depleted, respectively. Insets show the droplet thickness profiles at various spreading times (the vertical scale is 10 times larger than the horizontal one, for clarity). (b) Pressure difference and entanglement index (EI) versus time for Z ($N = 10$, $Q = 10\,000$). The insets show pressure maps (side view) and entanglement maps (top view) of the droplet. (c) Z molecules at the onset (left) and at the end (right) of spreading.

beads of the same molecule cause an $EI > 0$. The polymer molecules do not remain entangled because a molecule length of $N = 10$ is below the critical entanglement length, initially established for a primitive chain by Kremer et al.³⁶ and previously identified for our model as $N \approx 20$.^{32,37}

The insets in Figure 2b show the corresponding pressure (side view, averaged over 500 000 time steps) and entanglement (top view) maps (color scale provided). The pressure map insets depict an area of high pressure at the center base of the droplet at the inception of spreading, which creates a pressure difference that drives the molecules outward. The outer edges of the droplet show negative pressure, indicating that the outer molecules undergo tension. We attribute this to the van der Waals attraction between the polymer and substrate, which pulls the molecules outward.

We report the total pressure which is due mostly to disjoining pressure. We calculate the capillary component of the driving pressure difference at the beginning of the simulation using the radius of curvature of the central droplet and the surface tension. The capillary component comprises approximately 4% of the driving pressure difference for Z polymer with $N = 10$ and $Q = 10\,000$ and less than 10% for other cases. This indicates that the high pressure at the center of the droplet near the substrate is due mostly to molecular attraction between substrate and polymer liquid. The pressure within the central droplet drives the molecules to spread and neither entanglement nor chemical bonding to the substrate inhibits molecule motion. The pressure in the precursor film is due to disjoining pressure as the radius of curvature tends to infinity.

Figure 2c further illustrates the mechanisms identified in Figure 2b. We display one-quarter of the Z polymer droplet with $N = 10$ and $Q = 10\,000$ at the inception (left) and completion (right) of spreading, corresponding to the first and last data points of Figure 2a,b. Different shades of green depict different Z molecules except for two tagged molecules highlighted in red and blue, which we monitor during spreading. Black arcs correspond to the edge radius (outside the field of view for the right panel). From Figure 2c, we observe that the two short Z molecules entangle when spreading begins but untangle and separate by the end of the simulation.

Our simulations also indicate a significant slip of the polymer molecules over the substrate surface during spreading. Thus, while spreading may behave like pressure-driven continuum flow, it occurs without the zero slip condition at the liquid–solid interface commonly used for analyzing continuum flow. Figure S2 shows lubricant displacement maps at the beginning and end of the simulation for each spreading scenario and indicates significant wall slip of the precursor film for the case of pressure-driven flow. This agrees with previously reported velocity profiles that indicate slip of the precursor film at the substrate interface.³² We also note that our observation of $\nu \approx 1/3$ is in agreement with the theoretical predictions of Liao et al.¹⁸ for a precursor film spreading from a droplet in the case of continuum flow driven by disjoining pressure and with intensive slip at the liquid–solid interface, the same conditions verified in our simulations.

We point out that once the central droplet has depleted, the spreading exponent remains $\nu \approx 1/3$ for these short polymer molecules ($N = 10$), in contrast with longer chain polymers discussed next where spreading speed slows dramatically once the central droplet and the corresponding pressure difference depletes. For these short polymer molecules, one may expect molecular diffusion with $\nu \approx 0.5$ to dominate spreading once the backing pressure from the central droplet dissipates. Presumably, even though the polymer molecules are untangled at this stage, there are still sufficient molecule-to-molecule

interactions to inhibit regular Brownian motion diffusion, leading to the slower $\nu \approx 1/3$ exponent.

Pressure-Driven, Entanglement Inhibited Flow. Figure 3 illustrates spreading of a Z polymer droplet, a Zdol droplet with $S_f = 0\%$, and a Zdol droplet with $S_f = 100\%$, where $N =$

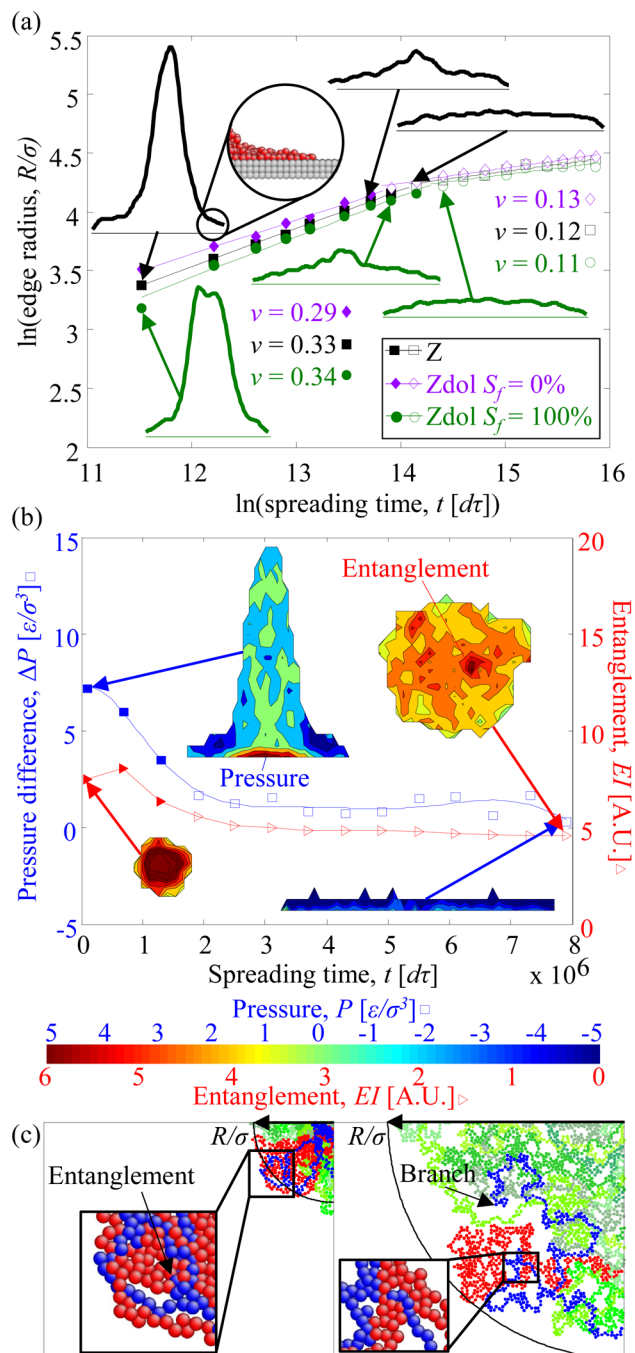


Figure 3. Pressure-driven, entanglement inhibited flow. (a) Edge radius versus spreading time for Z, Zdol with $S_f = 0\%$, and Zdol with $S_f = 100\%$ ($N = 400$ beads/molecule, $Q = 10\,000$ polymer beads). Solid and hollow markers indicate that a central droplet exists or has depleted, respectively. Insets show the droplet thickness profiles at various spreading times (the vertical scale is 10 times larger than the horizontal one, for clarity). (b) Pressure difference and entanglement index (EI) versus time for Z ($N = 400$, $Q = 10\,000$). The insets show pressure maps (side view) and entanglement maps (top view) of the droplet. (c) Z molecules at the onset (left) and after (right) spreading.

400 beads/molecule and $Q = 10\,000$ polymer beads. Figure 3a shows the droplet edge radius as a function of time during spreading, while the insets show the droplet thickness profiles and a molecular view of the precursor film that spreads to a thickness of less than 3σ . From Figure 3a, we observe that two regimes describe the droplet edge radius during spreading: an initial fast regime where $\nu = 0.29\text{--}0.34 \approx 1/3$ and, subsequently, a slower regime where $\nu = 0.11\text{--}0.13 \approx 1/10$. As illustrated by the droplet thickness profile insets, we observe that the transition in spreading speed occurs when the central droplet depletes. This agrees with observations by Mate,^{19,20} Kim et al.,²³ and Hardy³⁸ who show the importance of the central droplet in spreading, and Heslot et al.^{15,14} who observe that the central droplet acts as a limited-volume reservoir, emptied when the droplet completely wets. It is also in agreement with results presented by Wei et al.³⁹ that relate line tension of a single adsorbed polymer to spreading. As discussed next, unlike with short molecules, entanglement causes spreading to slow when the pressure in the central droplet no longer drives the molecules outward.

We note that the slower spreading regime is similar to that predicted by Tanner's law, despite the different physical mechanisms driving spreading in these two cases. From Figure S2, we observe that spreading is slow for cases that exhibit minimal wall slip. Since Tanner's law assumes no wall slip, we believe that this is the reason spreading is similar for these cases.

Figure 3b shows the pressure difference and entanglement index as a function of time within a droplet of Z polymer with $N = 400$ and $Q = 10\,000$. From Figure 3b, we observe that the droplet pressure difference decreases after spreading starts and, after the central droplet depletes, the pressure difference does not change by more than approximately $1 \text{ e}/\sigma^3$, indicating the droplet is reaching close to an equilibrium pancake shape, in agreement with De Gennes et al.⁹ At the onset of spreading, the inset shows an area of high pressure within the central droplet, which creates a pressure difference that drives the molecules outward and disappears as soon as the central droplet depletes.

We also observe that the EI is large at the inception of spreading because a cylinder initially confines the polymer, but, when allowed to spread, the EI decreases to approximately $EI \approx 5$. We observe that the EI decreases slower and remains larger than for short molecules (comparing to Figure 2b, where short molecules take less than $0.5 \times 10^6 \text{ d}\tau$ for the EI to reach a steady state of approximately 4). At the inception of spreading, the inset shows that the entire droplet entangles, but at the end of the simulation, the inset shows that the EI is larger throughout the droplet compared to short molecules and also reveals that local regions of very high entanglement remain at the end of the simulation, indicated by dark red regions not observed in Figure 2b. This depicts where molecules cross and entangle, which slows spreading in the absence of a pressure difference caused by the central droplet.

Figure 3c further illustrates the mechanism of polymer spreading. We display one-quarter of the Z polymer droplet with $N = 400$ and $Q = 10\,000$ at the inception (left) and completion (right) of spreading, corresponding to the first and last data points of Figure 3a,b, where black arcs correspond to the edge radius. From Figure 3c, we observe two long Z molecules that loop around and through each other and themselves at the beginning of the simulation. These molecules tightly entangle at the beginning of the simulation and remain largely intertwined at the end of the simulation. We notice,

however, that spreading causes the ends of the molecules to untangle although the center portions of the molecules remain tangled. We qualitatively refer to these untangled ends as branches that stretch away from the entangled droplet center. Entangled regions form in the center of the droplet, but the branches constrict and stretch away from the entangled regions, spreading only a finite distance as the middle region of the molecule remains largely entangled and immobile. In the case of long Zdol molecules ($N = 400$) functional end beads attract to the substrate, but since only 0.5% of the long Zdol molecule is functional, the nonfunctional backbone beads inhibit functional polymer end beads from attracting other functional polymer end beads or functional substrate beads, resulting in spreading that is almost identical to that of long Z molecules. Thus, for long molecules, the spreading kinetics is independent of polymer type and substrate functional fraction, indicating that molecular entanglement is a dominant mechanism that governs spreading of long molecules.

Pressure-Driven, Chemically Inhibited Flow. Figure 4 illustrates spreading of a liquid Zdol droplet with $S_f = 100\%$, $N = 10$ beads/molecule, and $Q = 10\,000$ polymer beads. Figure 4a shows the droplet edge radius as a function of time as it spreads, while the insets show the droplet thickness profiles and a molecular view of the spreading front. From Figure 4a, we observe that the central droplet does not deplete within the simulation duration, and only a slow spreading speed of $\nu = 0.16$ occurs. Because 20% of the short Zdol polymer molecules ($N = 10$) is functional and, thus, can attach to the fully functional substrate, many molecules pin in place, which severely constrains polymer motion. This agrees with the observations by Min et al.,¹⁷ Mate,²⁰ and Noble et al.³⁷ that spreading slows with increasing number of hydroxyl groups. Although pressure in the central droplet drives spreading, the attraction of functional groups to the substrate is the dominant mechanism inhibiting flow. Hence, we observe that the spreading exponent can also be sensitive to changes in the liquid–solid interaction as opposed to the liquid–liquid interaction, which is in agreement with experiments by Leleh et al.²¹

Figure 4b shows the pressure difference and entanglement within a droplet as a function of time for Zdol with $N = 10$ and $Q = 10\,000$. From Figure 4b, we observe that the droplet pressure difference remains high throughout the simulation because the molecular end groups constrain spreading, so that the central droplet and the area of high pressure caused by it do not deplete during the simulation. We also observe that the EI is high at the inception of spreading and increases slightly with time due to the functional end beads attracting each other and locally forming regions of high end bead density, which we refer to as end bead clusters.^{32,37} The insets show that the polymers are clustered at the beginning and end of the simulation, except within the precursor foot, which agrees with the simulations by Albrecht et al.²⁴ that document entangled molecules in the central part of the droplet, whereas outer molecules become progressively free.

In Figure 4c we display one-quarter of the droplet for Zdol with $N = 10$ and $Q = 10\,000$ at the inception (left) and completion (right) of spreading, corresponding to the first and last data points of Figure 4a and b, where black arcs correspond to the edge radius. From Figure 4c, we observe two short Zdol molecules that entangle at the beginning of the simulation. Clusters of functional end beads, which we indicate with an extra black circle (solid black in insets), form in the center

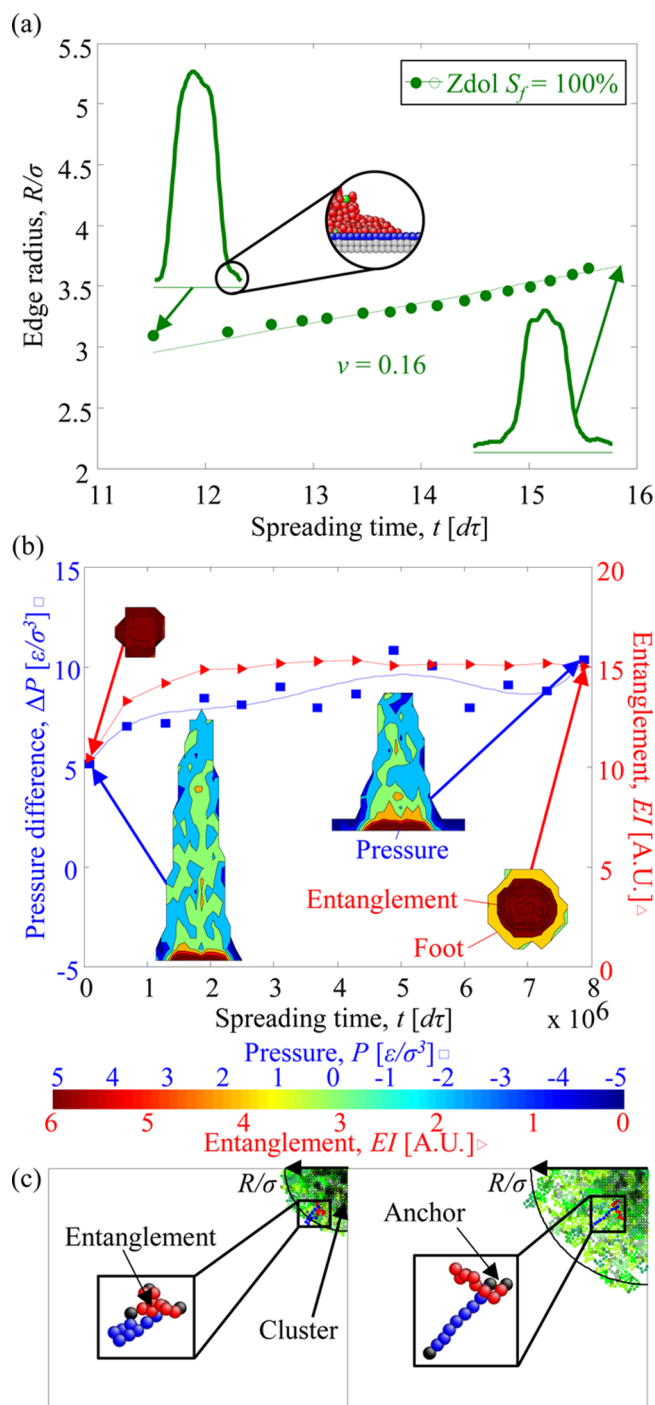


Figure 4. Pressure-driven, chemically inhibited flow. (a) Edge radius versus spreading time for Zdol ($S_f = 100\%$, $N = 10$ beads/molecule, $Q = 10\,000$ polymer beads). Solid and hollow markers indicate that a central droplet exists or has depleted, respectively. Insets show the droplet thickness profiles at various spreading times (the vertical scale is 10 times larger than the horizontal one, for clarity). (b) Pressure difference and entanglement index (EI) versus time. The insets show pressure maps (side view) and entanglement maps (top view) of the droplet. (c) Zdol molecules at the onset (left) and after (right) spreading; functional end groups are indicated with a black circle (solid black in insets).

region of the droplet due to the attraction of functional polymer end beads to each other and to the functional substrate beads. The location of the tagged molecules does not change

throughout the simulation because the functional end beads attach to functional substrate beads, inhibiting spreading. At the end of the simulation, we observe that the blue molecule stretches away from the droplet center but cannot spread freely because one functional bead pins to the substrate, which inhibits slip and, thus, the theoretical predictions of Liao et al.¹⁸ do not hold. Thus, in the case of short Zdol molecules spreading on a functional substrate, the attraction of functional end beads to each other and to the substrate is the dominant mechanism, and almost completely inhibits polymer spreading despite the pressure created by the presence of a central droplet, which results in a constant, slow spreading exponent $\nu \approx 1/10$.

Comparison to Experiments. We further justify these results in the context of previous experiments of liquid spreading. Our results agree closely with those obtained by Mate,^{19,20} likely because we study similar polymers and a similar range of molecular weights. Our results also qualitatively agree with Wang et al.^{40,41} who observed a slow spreading mechanism $\nu \approx 0.1$ for partially wetting liquids in the later stages of spreading and with Lelah et al.²¹ who measured spreading exponents mostly within the range $\nu = 0.10$ – 0.15 but as high as $\nu \approx 0.32$ and as low as $\nu \approx 0.03$. The majority of the spreading exponents we obtain in our simulations are within the range $\nu = 0.10$ – 0.16 , but we observe values as high as $\nu = 0.38$. We do not observe a very slow mechanism, i.e., $\nu < 0.1$, but we have shown previously that for very short, functional molecules, almost no spreading occurs because the functional groups cluster and no other driving mechanism is sufficiently strong to break the clusters.³⁷

Rafai et al.⁴² only observed a slow spreading exponent, but used very high molecular weight polymers, corresponding to $N \approx 20\,000$ in our simulations. We observe, however, that for $N = 400$, molecular entanglement slows spreading significantly, and for extremely long molecules this effect may be even more pronounced such that only a slow spreading speed occurs. Ma et al.¹⁵ and Min et al.¹⁷ used polymers and molecular weights similar to those studied in our simulations, but they observed a faster $\nu \approx 0.5$ spreading exponent. However, Ma et al. and Min et al. did not use droplets in the experiments; instead, the substrates were partially dip coated. This approach limits spreading to one direction and supplies a very large reservoir with a high-pressure region to drive spreading. O'Connor et al.²² also used the partial dip coating technique and, correspondingly, observed very fast spreading exponents of $\nu \approx 1.0$ followed by $\nu \approx 0.5$. The results obtained by O'Connor et al. were similar for both Z and Zdol. Our simulations attribute this to the bare silicon wafer used by O'Connor et al., which had no functional groups, whereas Min et al. reported slower spreading for functional polymer on modified silicon wafers with bonded Zdol, similar to our observations of Zdol spreading on a functional surface.

The height of the droplets in our simulations is a few nanometers, similar to droplets studied in experiments.^{15,17,19,20,22} However, the droplet volumes in our simulations (on the order of 10^{-21} L) are several orders of magnitude less than those typically used in experiments ($2\text{ fL} - 25\text{ }\mu\text{L}$),^{19–21,40–42} which may be a source of discrepancy. Figure S3 in the SI shows that the spreading exponent increases with increasing droplet volume, especially for short, nonfunctional molecules. We anticipate that the spreading speed may approach $\nu \approx 0.5$ with larger volume droplets.

CONCLUSIONS

The leading edge of a liquid polymer droplet advances as a power law $R \sim t^\nu$ with two successive regimes, one fast $\nu = 0.27$ – 0.38 and one slow $\nu = 0.10$ – 0.16 , which we attribute to competing mechanisms: a pressure difference in the droplet and entanglement of polymer molecules. This is similar to continuum flow of a liquid where the flow rate is dependent on the local pressure difference and inversely proportional to the effective viscosity, and contrasts with earlier reports that identify diffusion as the main spreading mechanism.

Our simulations can be used to predict the spreading behavior of an ultrathin polymeric liquid film based on the molecular weight, quantity, and chemical groups of the polymer. If a central droplet exists to feed polymer into the precursor film, pressure drives spreading and a fast mechanism occurs. However, if the central droplet depletes, the driving pressure difference vanishes and may cause spreading to slow. Molecular weight, or molecule length, directly influences polymer spreading as follows:

Long molecules spread quickly during the initial stages of spreading driven by the pressure difference caused by the central droplet. However, long molecules constrict around entangled regions, inhibiting spreading after the central droplet depletes.

Small molecules spread rapidly regardless of the presence of the central droplet, because no mechanism inhibits their motion, but still with a lower spreading exponent than expected for molecular diffusion ($\nu \approx 1/3$ vs $\nu \approx 0.5$).

Functional groups of the polymer and substrate also greatly affect spreading. Functional polymer groups attract each other and functional substrate groups, causing the molecules to cluster and to pin to the substrate, inhibiting spreading. For short molecules with functional end groups, this mechanism can be dominant and greatly slow spreading despite the presence of a central droplet, particularly if the substrate is also functional, allowing most molecules next to the substrate to become pinned.

METHODS

We use a time step of 0.03 ps throughout all MD simulations. First, the polymer equilibrates within a cylinder of diameter 23 nm for at least 7 ns, which represents the pipet in experiments to deposit a droplet on a substrate. We use a quasi-random distribution⁴³ to determine the initial position of the first bead of every molecular chain, and base the initial position of the additional beads belonging to each molecular chain on a random walk approach, starting from the first bead. We remove the cylinder at time $t = 0$, and the polymer spreads on a flat substrate for 250 ns. The polymer is free to move according to the microcanonical ensemble, and the temperature of the model is constant at 300 K using a Langevin thermostat. The substrate remains rigid throughout the simulation and periodic boundary conditions exist in the x - and z -directions (see coordinate system in Figure 1) although the polymer does not cross any boundary during any simulation in this work.

We quantify the spreading speed of the droplet by fitting the smallest circle that encompasses every polymer bead, iteratively converging on a final circle radius until exclusion of the outlying beads changes the radius by less than 10%. We fit a straight line through the natural logarithm of the radius of this circle as a function of the natural logarithm of the corresponding spreading time, where the slope represents the power law spreading exponent. We obtain the droplet profile by low-pass filtering the maximum value of the polymer y -coordinate (cutoff frequency of 0.1 [1/nm], based on spectral analysis) as a function of the x -coordinate (see coordinate system in Figure 1), in which the vertical scale is 10 times larger than the horizontal one,

for clarity. We calculate pressure by summing the negative trace of the per-bead stress tensor for all polymer beads in the simulation divided by the droplet volume and the number of diagonal terms (three dimensions in our simulations). We obtain local pressure maps (side view with vertical scale 10 times larger than the horizontal one, for clarity) by averaging along the radial coordinate over 500 000 time steps. We quantify the pressure difference by subtracting the pressure of the innermost 20% and outermost 20% of polymer near the substrate (less than 3σ in thickness). We also quantify entanglement by averaging the number of close (2σ), persistent (100 000 time steps) contacting beads for each bead in the simulation, similar to the definition of entanglement by Likhtman et al.³⁵ We obtain local entanglement maps employing the same method.

■ ASSOCIATED CONTENT

Supporting Information

The Supporting Information is available free of charge on the ACS Publications website at DOI: 10.1021/acs.langmuir.7b00334.

Schematic of potential functional interactions; lubricant displacement maps; effect of droplet volume; spreading exponents for Z lubricant, Zdol lubricant with $S_f = 100\%$, and Zdol lubricant with $S_f = 0\%$ (PDF)

Pressure-driven flow (AVI)

Pressure-driven, entanglement inhibited flow (AVI)

Pressure-driven, chemically inhibited flow (AVI)

■ AUTHOR INFORMATION

Corresponding Author

*E-mail: bart.raeymaekers@utah.edu.

ORCID

Bart Raeymaekers: 0000-0001-5902-3782

Present Address

#C.M.M., 1672 Hester Avenue, San Jose, CA 95128, United States.

Notes

The authors declare no competing financial interest.

■ ACKNOWLEDGMENTS

Brooklyn Noble gratefully acknowledges the Department of Energy Stewardship Science Graduate Fellowship program support, provided under grant number DE-NA0002135. This work used the Extreme Science and Engineering Discovery Environment (XSEDE), which is supported by National Science Foundation grant number ACI-1053575, and the support and resources from the Center for High Performance Computing at the University of Utah are also gratefully acknowledged.

■ REFERENCES

- (1) De Gennes, P. G.; Brochard-Wyart, F.; Quéré, D. *Capillarity and wetting phenomena: drops, bubbles, pearls, waves*; Springer Science & Business Media: 2013.
- (2) Marchon, B. Lubricant design attributes for subnanometer head-disk clearance. *IEEE Trans. Magn.* **2009**, *45*, 872–876.
- (3) Kim, S. H.; Asay, D. B.; Dugger, M. T. Nanotribology and MEMS. *Nano Today* **2007**, *2*, 22–29.
- (4) Baumchen, O.; Jacobs, K. Slip effects in polymer thin films. *J. Phys.: Condens. Matter* **2010**, *22*, 033102.
- (5) Epstein, A. K.; Wong, T.-S.; Belisle, R. A.; Boggs, E. M.; Aizenberg, J. Liquid-infused structured surface with exceptional anti-biofouling performance. *Proc. Natl. Acad. Sci. U. S. A.* **2012**, *109*, 13182–13187.
- (6) Teisseire, J.; Revaux, A.; Foresti, M.; Barthel, E. Confinement and flow dynamics in thin polymer films for nanoimprint lithography. *Appl. Phys. Lett.* **2011**, *98*, 013106.
- (7) Ku, I. S. Y.; Reddyhoff, T.; Holmes, A. S.; Spikes, H. A. Wear of silicon surfaces in MEMS. *Wear* **2011**, *271*, 1050–1058.
- (8) Dussan, E. B. On the spreading of liquids on solid surfaces: static and dynamic contact lines. *Annu. Rev. Fluid Mech.* **1979**, *11*, 371–400.
- (9) De Gennes, P.-G. Wetting: statics and dynamics. *Rev. Mod. Phys.* **1985**, *57*, 827–863.
- (10) Tanner, L. H. The spreading of silicone oil drops on horizontal surfaces. *J. Phys. D: Appl. Phys.* **1979**, *12*, 1473.
- (11) De Gennes, P. G. *Introduction to polymer dynamics*; Cambridge University Press, 1990.
- (12) Xu, H.; et al. Molecular motion in a spreading precursor film. *Phys. Rev. Lett.* **2004**, *93*, 206103.
- (13) Feslot, F.; Cazabat, A. M.; Fraysse, N. Diffusion-controlled wetting films. *J. Phys.: Condens. Matter* **1989**, *1*, 5793–5798.
- (14) Heslot, F.; Cazabat, A. M.; Levinson, P. Dynamics of wetting of tiny drops: ellipsometric study of the late stages of spreading. *Phys. Rev. Lett.* **1989**, *62*, 1286–1289.
- (15) Ma, X.; Tang, H.; Gui, J. Temperature effect on spreading of perfluoropolyethers on amorphous carbon films. *Tribol. Lett.* **2001**, *10*, 203–209.
- (16) Valignat, M. P.; Oshanin, G.; Villette, S.; Cazabat, A. M.; Moreau, M. Molecular weight dependence of spreading rates of ultrathin polymeric films. *Phys. Rev. Lett.* **1998**, *80*, 5377–5380.
- (17) Min, B. G.; et al. Spreading characteristics of thin liquid films of perfluoropolyalkylethers on solid surfaces. Effects of chain-end functionality and humidity. *Tribol. Lett.* **1995**, *1*, 225–32.
- (18) Liao, Y. C.; Li, Y. C.; Wei, H. H. Drastic changes in interfacial hydrodynamics due to wall slippage: slip-intensified film thinning, drop spreading, and capillary instability. *Phys. Rev. Lett.* **2013**, *111*, 136001.
- (19) Mate, C. M. Anomalous Diffusion Kinetics of the precursor film that spreads from polymer droplets. *Langmuir* **2012**, *28*, 16821–16827.
- (20) Mate, C. M. Spreading kinetics of lubricant droplets on magnetic recording disks. *Tribol. Lett.* **2013**, *51*, 385–395.
- (21) Lelah, M. D.; Marmur, A. Spreading kinetics of drops on glass. *J. Colloid Interface Sci.* **1981**, *82*, 518–525.
- (22) O'Connor, T. M.; et al. Surface diffusion and flow activation energies of perfluoropolyalkylether. *Tribol. Lett.* **1995**, *1*, 219–223.
- (23) Kim, S. J.; et al. Liquid spreading on superhydrophilic micropillar arrays. *J. Fluid Mech.* **2011**, *680*, 477–487.
- (24) Albrecht, U.; Otto, A.; Leiderer, P. Two-dimensional liquid polymer diffusion: experiment and simulation. *Phys. Rev. Lett.* **1992**, *68*, 3192–3195.
- (25) De Coninck, J.; D'Ortona, U. Terraced spreading of chain molecules via molecular dynamics. *Phys. Rev. Lett.* **1995**, *74*, 928–931.
- (26) Heine, D. R.; Grest, G. S.; Webb, E. B., III Surface wetting of liquid nanodroplets: droplet-size effect. *Phys. Rev. Lett.* **2005**, *95*, 107801.
- (27) Samsonov, V. M.; Ratnikov, A. S. Comparative molecular dynamics study of simple and polymer nanodroplet spreading. *Colloids Surf., A* **2007**, *298*, 52–57.
- (28) Hsia, Y.-T.; Guo, Q.; Izumisawa, S.; Jhon, M. S. The dynamic behavior of ultrathin lubricant films. *Microsyst. Technol.* **2005**, *11*, 881–886.
- (29) Vinay, S. J.; et al. Simulation of ultrathin lubricant films spreading over various carbon surfaces. *J. Appl. Phys.* **2000**, *87*, 6164–6166.
- (30) Plimpton, S. Fast parallel algorithms for short-range molecular dynamics. *J. Comput. Phys.* **1995**, *117*, 1–19.
- (31) Towns, J.; et al. XSEDE: accelerating scientific discovery. *Comput. Sci. Eng.* **2014**, *16*, 62–74.
- (32) Noble, B. A.; Ovcharenko, A.; Raeymaekers, B. Terraced spreading of nanometer-thin lubricant using molecular dynamics. *Polymer* **2016**, *84*, 286–292.

- (33) Guo, Q.; Izumisawa, S.; Phillips, D. M.; Jhon, M. S. Surface morphology and molecular conformation for ultrathin lubricant films with functional end groups. *J. Appl. Phys.* **2003**, *93*, 8707–8709.
- (34) Chen, H.; Guo, Q.; Jhon, M. S. Effects of molecular structure on the conformation and dynamics of perfluoropolyether nanofilms. *IEEE Trans. Magn.* **2007**, *43*, 2247–2249.
- (35) Likhtman, A. E.; Ponmurugan, M. Microscopic definition of polymer entanglements. *Macromolecules* **2014**, *47*, 1470–1481.
- (36) Kremer, K.; Grest, G. S. Dynamics of entangled linear polymer melts: A molecular-dynamics simulation. *J. Chem. Phys.* **1990**, *92*, 5057–5086.
- (37) Noble, B.; Ovcharenko, A.; Raeymaekers, B. Quantifying lubricant droplet spreading on a flat substrate using molecular dynamics. *Appl. Phys. Lett.* **2014**, *105*, 151601.
- (38) Hardy, W. B. The spreading of fluids on glass. *Philos. Mag.* **1919**, *38*, 49–55.
- (39) Wei, H.-H.; Li, Y.-C. Conformational transitions of single polymer adsorption in poor solvent: Wetting transition due to molecular confinement induced line tension. *Phys. Rev. E: Stat. Phys., Plasmas, Fluids, Relat. Interdiscip. Top.* **2016**, *94*, 012501.
- (40) Wang, X. D.; Lee, D. J.; Peng, X. F.; Lai, J. Y. Spreading dynamics and dynamic contact angle of non-Newtonian fluids. *Langmuir* **2007**, *23*, 8042–8047.
- (41) Wang, X. D.; Zhang, Y.; Lee, D. J.; Peng, X. F. Spreading of completely wetting or partially wetting power-law fluid on solid surface. *Langmuir* **2007**, *23*, 9258–9262.
- (42) Rafai, S.; Bonn, D.; Boudaoud, A. Spreading of non-Newtonian fluids on hydrophilic surfaces. *J. Fluid Mech.* **1999**, *513*, 77–85.
- (43) Kocis, L.; Whiten, W. J. Computational investigations of low-discrepancy sequences. *ACM Trans. Math. Softw.* **1997**, *23*, 266–294.